Applied Catalysis B: Environmental 244 (2019) 529–535

Contents lists available at ScienceDirect

Applied Catalysis B: Environmental

journal homepage: www.elsevier.com/locate/apcatb

A facile method for regulating the charge transfer route of WO_3/CdS in high-efficiency hydrogen production

Lulu Zhang[a], Hongwen Zhang[a], Bo Wang[a], Xueyan Huang[a], Yun Ye[a], Rui Lei[a], Wenhui Feng[b,*], Ping Liu[a,*]

[a] Research Institute of Photocatalysis, State Key Laboratory of Photocatalysis on Energy and Environment, Fuzhou University, Fuzhou 350002, PR China
[b] Hunan Provincial Collaborative Innovation Center for Environment and Energy Photocatalysis, Changsha University, Changsha 410022, PR China

ARTICLE INFO

Keywords:
$H_{0.53}WO_3$/CdS
charge transfer route
type-II
Z-scheme
photochromism

ABSTRACT

In order to intrinsically boost the photocatalytic performance of WO_3/CdS, the charge transfer route can be modulated from conventional type-II to Z-scheme by incorporating of hydrogen ions into WO_3/CdS to form $H_{0.53}WO_3$/CdS. This work indicates that only when charge transfer of WO_3/CdS is type-II, can $H_{0.53}WO_3$/CdS composite be formed in-situ. Subsequently, the Z-scheme photocatalytic mechanism plays its prominent roles in gradually improving photocatalytic H_2 evolution performance. $H_{0.53}WO_3$/CdS has high photocatalytic activity for hydrogen production, which is much higher than that of WO_3/CdS. This work will provides an in-depth understanding of charge separation and transfer processes and steer charge flow in a Z-scheme manner for efficient solar-to-chemical energy applications.

1. Introduction

WO_3 has been applied in photocatalytic oxygen production [1,2] and degradation of some organic contaminants [3,4] because of its relatively positive valence band (VB) potential. However, its relatively positive conduction band (CB) potential restrict the reducing capacity of photogenerated electrons, which may lead to heavily recombination of photogenerated charge carriers [5,6]. Compounding with other semiconductors can be seen as an effective strategy for accelerating charge carriers separation [7,8]. In the categories of composite photocatalytic system, heterojunction-type-II, for instance, WO_3/CdS, is one of the most extensively concerned photocatalytic systems. Owing to the energy levels differences of two components, there are two possible transmitting ways of charge carriers in this hybrid, which are often referred to as conventional type-II [9–12]and Z-scheme [5–7]shown in the left and right of Fig.8, respectively. For WO_3/CdS, it indeed shows this two transmitting ways due to the different synthesis methods and reaction conditions [5,7,10,12].

As is known, in a conventional type-II photocatalytic system, the photogenerated electrons and holes are spatially isolated, which greatly inhibits their undesirable recombination. However, this advantage is at the cost of its low redox ability. Hence, such heterojunction-type photocatalytic system is almost impossible to simultaneously possess the ability of achieving double-efficient objective i.e. the high charge-separation efficiency and strong redox property [13,14]. In order to achieve this purpose, the artificial Z-scheme photocatalytic system is developed. In Z-scheme photocatalytic system, the photogenerated electrons and holes are also spatially isolated, as well as the strong redox ability can be achieved [15–17]. Consequently, how to make full use of conventional type-II system and modulate the charge transfer mode from conventional type-II to favor Z-scheme in the WO_3/CdS system can be an effective strategy for intrinsically boosting the photocatalytic performance [18,19].

In order to achieve the above project, adjusting the matched-degree of band structures is a feasible way. Lots of researches show that introducing defects into the photocatalytic system in certain degree can have influence on the band structures due to the impurity levels [20–24]. Inspired by this, if incorporation of hydrogen ions into WO_3, metastable hydrogen tungsten bronze can be formed, which is a series of non-stoichiometric materials with formula H_xWO_3 (x in the range from 0.1 to 0.6) [25,26]. Therefore, during the WO_3/CdS transforms into H_xWO_3/CdS, this process is accompanied by the change of matched-degree of band structures, which may be a potential way for modulating charge transfer route. However, there are few reports about applying H_xWO_3 into photocatalytic system [3], the main reason is that the preparation method of H_xWO_3 is demanding. In general, hydrogen tungsten bronzes can be prepared via thermal reduction [27], wet-chemical method [28] and electrochemistry method [29]. But these

* Corresponding author.
E-mail addresses: 380803116@qq.com (W. Feng), liuping@fzu.edu.cn (P. Liu).

https://doi.org/10.1016/j.apcatb.2018.11.055
Received 5 September 2018; Received in revised form 15 November 2018; Accepted 18 November 2018
Available online 19 November 2018
0926-3373/

methods have their own drawbacks – i.e. reducing gases consumption, specific reaction vessels and poor repeatability. Hence, in order to apply H_xWO_3 to the photocatalytic system, a facile method to synthesize H_xWO_3 is essential.

Based on the characteristics of WO_3, it exhibits photochromism under UV-light irradiation [30]. In this process, H_xWO_3 can be synthesized according to the equation: $WO_3 + x\ H^+ + x\ e^- \Leftrightarrow H_xWO_3$ [31–33]. However, this method is less efficient, and heavily-incorporated H_xWO_3 can be hardly obtained only by UV-light irradiation WO_3 due to its relatively poor reducibility of electrons [34]. While in the WO_3/CdS system, electrons from CdS that possess strong reducibility can transfer to WO_3, which is more easily to accelerate photochromism than pure WO_3. Therefore, it can be expected that H_xWO_3 can be synthesized efficiently and the corresponding charge transfer can be modulated.

Herein, in this work, hydrogen-incorporated WO_3/CdS ($H_{0.53}WO_3$/CdS) is successfully transformed by photochromism of WO_3/CdS and the corresponding charge transfer can be switched from conventional type-II to Z-scheme. Thanks to the Z-scheme mechanism, the photocatalytic H_2 evolution performance is improved dramatically. This work also indicates that $H_{0.53}WO_3$/CdS is easily restored to WO_3/CdS in the air and the performance is also decreased, but because of the type-II charge transfer during the reaction condition, WO_3/CdS can transform into H_xWO_3/CdS and the corresponding charge transfer follows Z-scheme again. Our current work is expected to offer new insight into the facile method for switching charge transfer from conventional type-II to Z-scheme and providing a potential way to achieve the aforementioned double-efficient objective.

2. Experimental section

2.1. Materials

WCl_6, $Cd(CH_3COO)_2{\cdot}2H_2O$, CH_4N_2S, n-Propanol, absolute ethanol, nitric acid (65-68 wt %) and lactic acid were obtained from Sinopharm Chemical Reagent Co., Ltd. (Shanghai, China). All the chemicals were of analytical grade and without further purification. Deionized (DI) water was used throughout this study.

2.2. Synthesis of photocatalysts

2.2.1. Preparation of WO_3

$W_{18}O_{49}$ was prepared by alcoholysis of WCl_6 according to literature [35] and used as precursor. Typically, 200 mg WCl_6 was dissolved in 50 mL n-Propanol, transferred to a Teflon-lined autoclave (100 mL) and heated at 200 °C for 24 h. The precipitate was collected via centrifugation, washed thoroughly with ethanol and H_2O. Then the produced $W_{18}O_{49}$ was put in a alumina crucible, heated at ramp rate of 10 °C/min, and finally held at 350 °C for 2 h in a muffle furnace to obtain WO_3.

2.2.2. Preparation of WO_3/CdS

WO_3/CdS composite was fabricated by chemical bath deposition [36]. 40 mg of WO_3 sample was added in 40 mL de-ionized water containing 1.48 g $Cd(CH_3COO)_2{\cdot}2H_2O$. Subsequently, the above suspension was stirred for 30 min in dark to achieve the preferential absorption of Cd ion on the surface of WO_3. 0.8 g CH_4N_2S was then added to the suspension. After the chemical bath deposition at 80 °C for 30 min, the precipitate was collected by centrifugation and washed with de-ionized water several times to remove dissolvable ionic impurities. The sample was dried at 60 °C in vacuum oven and named as WO_3/CdS.

2.2.3. Preparation of $H_{0.53}WO_3$/CdS

$H_{0.53}WO_3$/CdS was prepared through the following process. First, a certain amount of WO_3/CdS was dispersed in 100 mL aqueous solution containing 10 vol.% of lactic acid. Then the suspension was irradiated by a 300 W Xe lamp with a 420 nm cutoff filter for 30 min. The precipitate was collected by centrifugation and washed with de-ionized water several times to remove lactic acid. Finally sample was dried at 60 °C in vacuum oven.

2.2.4. Preparation of CdS

CdS was synthesized by the method similar to WO_3/CdS but without adding WO_3.

2.2.5. Preparation of $H_{0.53}WO_3$

A certain amount of $H_{0.53}WO_3$/CdS was dispersed in 300 mL aqueous solution containing 25 vol.% of concentrated HNO_3. After 30 min stirring at room temperature, the precipitate was collected by centrifugation and washed with de-ionized water. The sample was dried at 60 °C in vacuum oven.

2.2.6. Preparation of WO_3-L and CdS-L

WO_3-L and CdS-L were synthesized through putting WO_3 and CdS into lactic acid under illumination respectively, which is similar to the preparation of $H_{0.53}WO_3$/CdS.

2.2.7. Preparation of $H_{0.53}WO_3$/CdS-R

$H_{0.53}WO_3$/CdS-R was synthesized by stirring $H_{0.53}WO_3$/CdS in the air for 24 h.

2.3. Characterization

The crystallographic properties of the as-prepared samples were measured on a Bruker D8 ADVANCE X-ray diffractometer with Cu Kαradiation (l = 0.15418 nm), which operated at 40 kV and 40 mA. The scan rate is 0.5 ($2\theta{\cdot}s^{-1}$). Scanning electron microscopy (SEM) images are obtained using a HITACHI SU8000 field-emission scanning electron microscope. The transmission electron microscopy (TEM) analysis of the samples was taken using a transmission electron microscope (TEM, FEI Tecnai G20) at an accelerating voltage of 200 kV. UV–vis diffuse reflectance spectroscopy (DRS) was measured by a Carry 500 UV–vis spectrophotometer, during which $BaSO_4$ was served as the background. The nitrogen adsorption and desorption isotherms were characterized using a Micrometrics ASAP 2020 analyzer at 77 K after the as-prepared samples were degassed at 180 °C for 300 min in a vacuum. X-ray photoelectron spectroscopy (XPS) investigation was recorded on a Thermo Scientific ESCA Lab 250 system, with a monochromatic Al Kα as the X-ray source, hemispherical analyzer, and sample stage with multi-axial adjustability to obtain the composition on the surface of samples. The BAS Epsilon workstation is utilized to monitor the open circuit potential of samples. The working electrode is prepared on fluoride tin oxide (FTO) conductor glass. Typically, 10 mg sample powder is mixed with 1 mL DMF to make slurry. The slurry is then spread onto the FTO glass, whose side part is previously protected using 95 Scotch tapes. The working electrode is further dried at 100 °C for 3 h to improve adhesion. 0.2 M of aqueous Na_2SO_4 solution is used as the supporting electrolyte.

2.4. Photocatalytic hydrogen evolution

The photocatalytic activity was evaluated with 30 mg photocatalyst suspended in 100 mL aqueous solution containing 10 vol.% of lactic acid as the sacrificial agent, which performed in a relatively vacuum system allocated an external glass reaction cell by the Labsolar-6 A photocatalytic water decomposition hydrogen production system (Prefect light company). The suspension was sealed in a quartz vessel, sonicated for 10 min and purged with argon gas for 60 min to remove all air in solution and headspace. After degassing, the vessel was vertically irradiated by a 300 W Xe lamp (PLS-SXE 300/300UV, Beijing Perfect light Technology Co. Ltd.) coupled with a UV cut-off filter

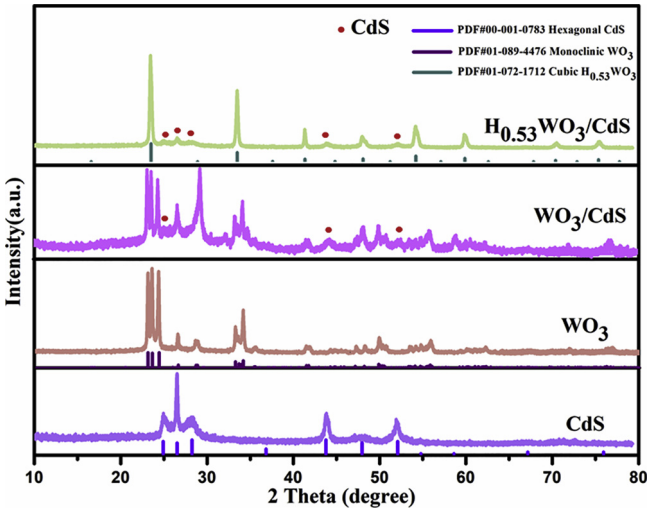

Fig. 1. XRD patterns of CdS, WO_3, WO_3/CdS and $H_{0.53}WO_3$/CdS.

(λ ≥ 420 nm). The temperature of reaction solution was maintained at 5 °C. The amount of generated H_2 was analyzed by a gas chromatograph (Bruker 450-GC) with a thermal conductivity detector (TCD, molecular sieve 5 A, argon carrier gas 99.999%).

3. Results and discussion

3.1. Characterizations of photocatalysts

In the designed synthesis process, WO_3/CdS should gradually transform into $H_{0.53}WO_3$/CdS under illumination. Hence, the structural characterization of samples is of vital importance. XRD investigation is performed to explore the crystal structure and phase of as-synthesized materials. As shown in Fig.1, the sharp peak patterns of CdS and WO_3 are well matched with the standard Joint Committee on Powder Diffraction Standards (JCPDS) card No. 00-001-0783 and No. 01-089-4476, which is assigned to hexagonal CdS and monoclinic WO_3, respectively. Besides, it is obvious that the composite of WO_3/CdS is successfully synthesized. The composite of $H_{0.53}WO_3$/CdS is successfully synthesized by photochromism of WO_3/CdS, which is composed of cubic $H_{0.53}WO_3$ (No. 01-072-1712) and hexagonal CdS. No characteristic peaks of any impurities are detected.

SEM characterization is applied to obtain more detailed structural information of all prepared samples. As shown in Fig. 2a, pure WO_3 shows short rods with a diameter of 150 nm and a length of 200-500 nm and relatively smooth surface. After depositing CdS particles, as shown in Fig. 2c, the surface of WO_3/CdS composites becomes rough, which indicates that crystallized CdS nanoparticles grow onto the surfaces of WO_3 to form the hybrid. In addition, the morphology of $H_{0.53}WO_3$/CdS shown in Fig. 2d, which is similar to WO_3/CdS, indicating that introducing defects into WO_3/CdS has no obvious affection in the morphology.

TEM investigation is applied to further confirm the crystal structures and morphologies of WO_3/CdS and $H_{0.53}WO_3$/CdS. It is found from Fig. 3 that the CdS nanoparticles do be deposited on the WO_3 and $H_{0.53}WO_3$ hosts, respectively. As shown in Fig.3b (Partially enlarged view of Fig. 3a), High-resolution TEM (HRTEM) image shows the characteristic spacing of 0.336 nm, corresponding to the (002) lattice plane of wurtzite CdS. Simultaneously, the lattice fringes of WO_3 display interplanar spacing of 0.366 and 0.386 nm, which matches well with the (200) and (002) planes of the monoclinic WO_3, respectively. Fig.3d shows the characteristic spacing of 0.336 and 0.355 nm, corresponding to the (002) and (100) lattice plane of wurtzite CdS, respectively. Simultaneously, the lattice fringes of $H_{0.53}WO_3$ display interplanar spacing of 0.378 nm, which matches well with the (200) planes of the cubic $H_{0.53}WO_3$. Both TEM and HRTEM images confirm that hydrogen ions are successfully incorporated into WO3/CdS, which are consistent with the results of XRD and SEM.

XPS investigation is a powerful evidence for further verifying the transformation of WO_3 into $H_{0.53}WO_3$. As shown in Fig.4a, the dominant peaks at 37.3 and 35.2 eV are corresponded to W^{6+} ions in WO_3/CdS. However, there are five peaks in $H_{0.53}WO_3$/CdS shown in Fig.4b. The W-4f peaks become broader after photochromism. This indicates that the tungsten in the coloration may be present multiple valence states. The dominant peaks at 37.7 and 35.4 eV are correspond to W^{6+} ions [37], the lesser peaks at 36.4 and 34.1 eV are ascribed to W^{5+} ions, 35.4 eV and 33.1 eV are ascribed to W^{4+} ions in the lattice [33,38–41], respectively. Comparing the transformation of XPS peaks in Figs. 4a and 4b, it is not difficult to conclude that WO_3/CdS in aqueous solution has been transformed into $H_{0.53}WO_3$/CdS under illumination. Besides, According to the O 1 s XPS spectra of $H_{0.53}WO_3$/CdS shown in Fig.S1, the peak at 533.1 eV is correspond to -OH groups, while there is no peak at ~533 eV for the O 1 s XPS spectra of WO_3/CdS, which also indicates that hydrogen ions are successfully incorporated into WO_3/CdS.

3.2. Photocatalysis

The photocatalytic H_2 evolution performances of aforementioned products are evaluated under visible light irradiation (λ ≥ 420 nm) as shown in Fig. 5. Pure CdS shows very low activity (0.026 mmol $h^{-1} g^{-1}$) due to rapid recombination of photoinduced charge carriers. WO_3 is almost inactive owing to its too positive conduction band. Similarly, the activity of $H_{0.53}WO_3$ is so low that it cannot be detected. Nevertheless, $H_{0.53}WO_3$/CdS composite exhibits a much higher activity of H_2 production than that of either $H_{0.53}WO_3$ or CdS individually. Curiously, the activity of H_2 production is weak (0.82 mmol $h^{-1} g^{-1}$) in the first hour, and the H_2 production rate is increased in the first fourth hours. One possible reason is that the increased content of $H_{0.53}WO_3$ in $H_{0.53}WO_3$/CdS along with the light irradiation, traditional type-II photocatalytic mechanism and Z-scheme photocatalytic mechanism sequentially acts. First, under the influence of heterojunction-type photocatalytic mechanism, $H_{0.53}WO_3$/CdS is gradually forming in the first four hours. In this process, the sample consists of a mixture of WO_3/CdS and $H_{0.53}WO_3$/CdS. And its relatively low activity is attributed to type-II photocatalytic mechanism of WO_3/CdS. After 4 hours, WO_3/CdS almost changes to $H_{0.53}WO_3$/CdS. And $H_{0.53}WO_3$/CdS follows the Z-scheme photocatalytic mechanism to separate and transfer photogenerated carriers, which can increase its performance. At this time, its hydrogen evolution activity is as high as 2.94 mmol $h^{-1} g^{-1}$. During the photocatalytic H_2 evolution, WO_3/CdS can be transformed into $H_{0.53}WO_3$/CdS gradually, therefore, the activity of the first four hours is a result of the mixture. Owing to the high performance of $H_{0.53}WO_3$/CdS, it can be concluded that WO_3/CdS shows fairly low activity.

The stability is among the most important aspects for photocatalysts. Notably, as shown in Fig. S3. In order to as full formed $H_{0.53}WO_3$/CdS as possible, before the cycle experiment, $H_{0.53}WO_3$/CdS has been light irradiated for 6 h. As shown in Fig. S3, $H_{0.53}WO_3$/CdS present a satisfying stable performance of hydrogen production during a 15 h cycling test without refreshing the catalysts and sacrificial agents. This result implies that Z-scheme mechanism in $H_{0.53}WO_3$/CdS can restrain CdS from photo-corrosion during the photocatalytic process, leading to the excellent photocatalytic stability.

In order to understand the reasons for the enhanced photocatalytic capability of the $H_{0.53}WO_3$/CdS under visible light irradiation, the Optical properties of the as-prepared samples have been investigated via UV-vis diffuse reflectance spectroscopy (DRS) shown in Fig. 6a. It can be clearly seen that the adsorption band edge of WO_3/CdS is blue shifted compared with CdS. In all samples, $H_{0.53}WO_3$/CdS has a broader absorption in visible light region and higher absorption intensity

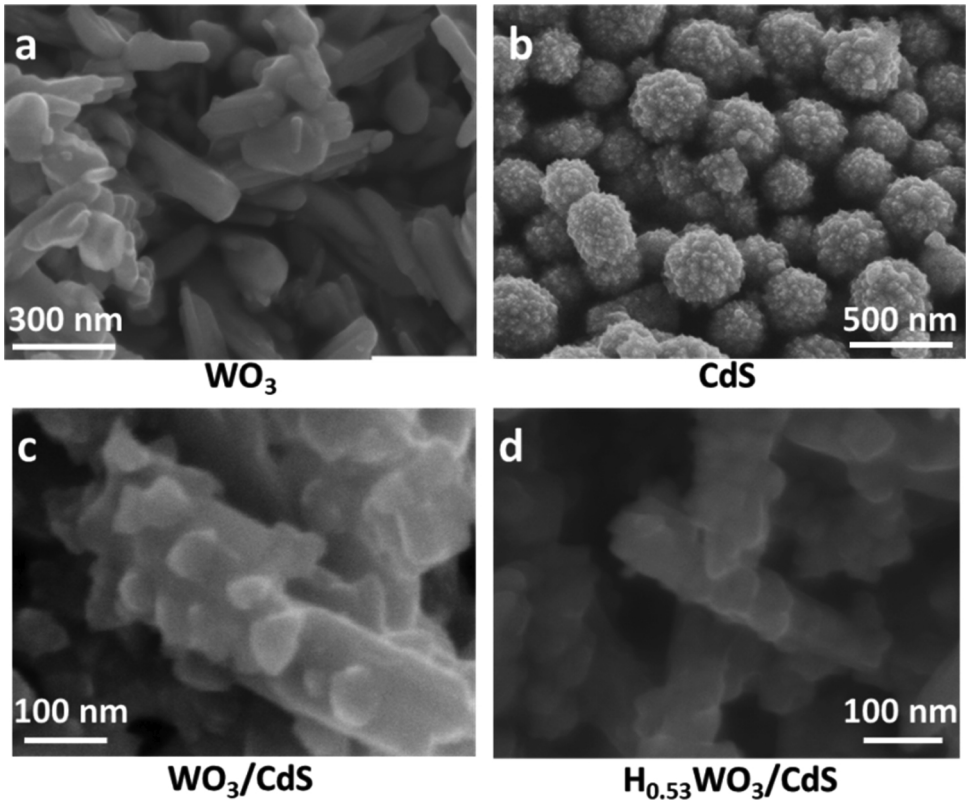

Fig. 2. SEM patterns of the samples (a) WO_3, (b) CdS, (c) WO_3/CdS, (d) $H_{0.53}WO_3$/CdS.

compared with WO_3/CdS owing to photochromic effect of WO_3, which indicates that more charge carriers can be generated for improving the performance. Although $H_{0.53}WO_3$ also has a broader absorption in visible light region, its photocatalytic performance is too poor to be detected, which is mainly attributed to the relatively positive CB. Fig. 6b shows the typical photographs of the WO_3/CdS, $H_{0.53}WO_3$/CdS and $H_{0.53}WO_3$/CdS-R photocatalyst samples, which can be observed clearly that the suspension containing WO_3/CdS turns its color from a

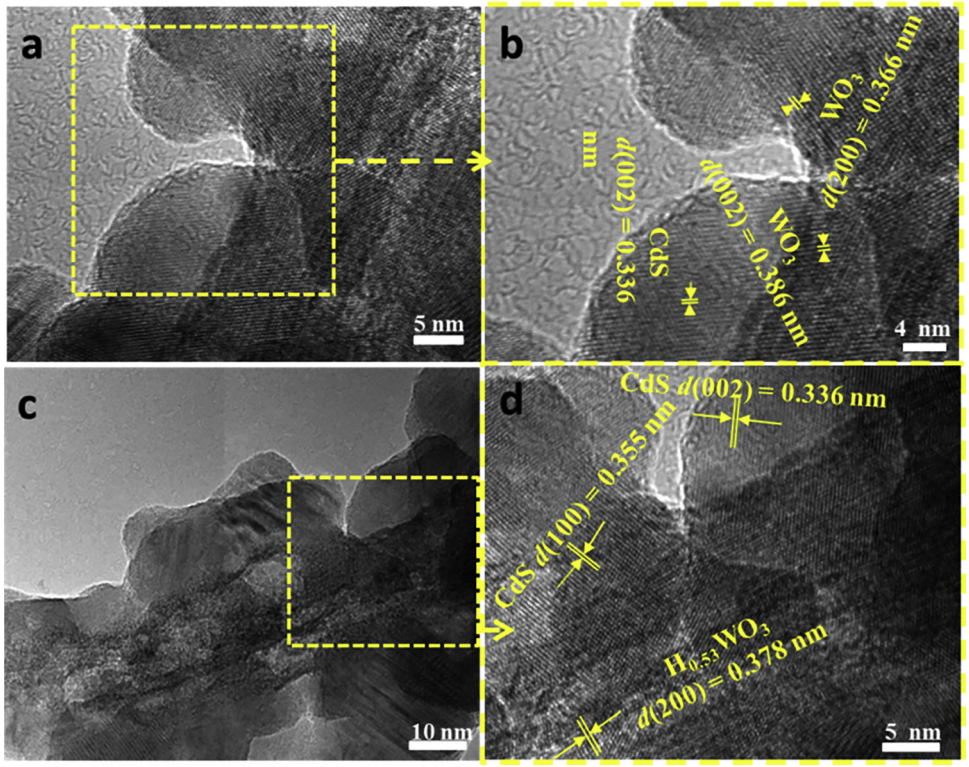

Fig. 3. TEM patterns of the sample (a,b) WO_3/CdS and (c,d) $H_{0.53}WO_3$/CdS.

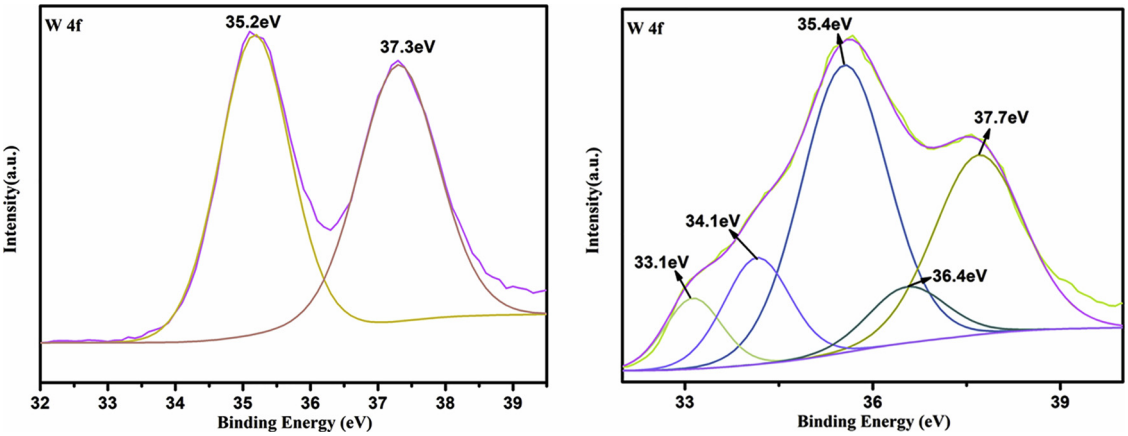

Fig. 4. W 4f XPS spectra of (a) WO_3/CdS and (b) $H_{0.53}WO_3$/CdS.

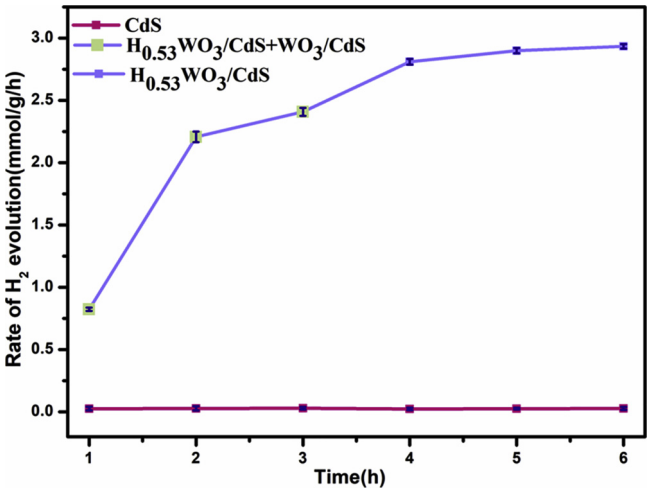

Fig. 5. Photocatalytic H_2 evolution rates of all samples under visible light irradiation ($\lambda \geq 420$ nm).

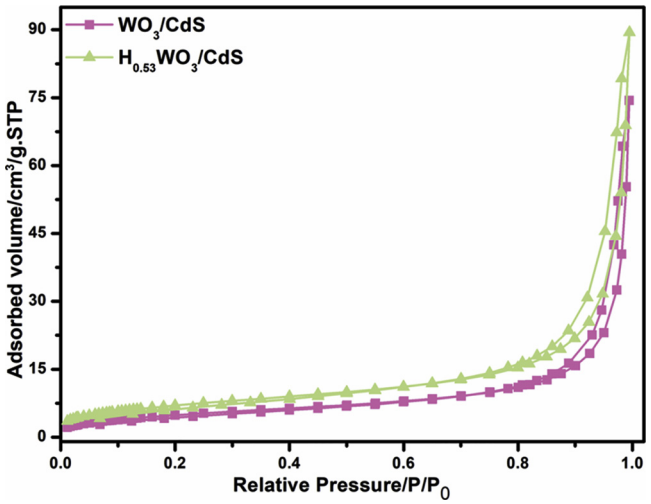

Fig. 7. Nitrogen adsorption desorption isotherms of WO_3/CdS and $H_{0.53}WO_3$/CdS.

bright yellow to deep blue after illumination. As the illumination time increases, the absorption intensity in visible light region gradually improves. When exposed to the air, $H_{0.53}WO_3$/CdS is easily oxidized to WO_3/CdS, which can be evidenced by XRD, as shown in Fig. S3, the XRD pattern of $H_{0.53}WO_3$/CdS-R is in accordance with WO_3/CdS.

As the specific surface area is one of the important factors that affect the activity of the photocatalysts, the BET surface areas of the photocatalysts are investigated by nitrogen adsorption–desorption. The BET specific surface areas of the samples increase from 14.2 $m^2 g^{-1}$ (WO_3/CdS) to 25.2 $m^2 g^{-1}$ ($H_{0.53}WO_3$/CdS) after incorporation of hydrogen ions (Table S1 and Fig. 7). Although the BET specific surface area of $H_{0.53}WO_3$/CdS is about 2 times than that of WO_3/CdS, the performance is more than 9 times. Therefore, increased BET specific surface area is not the main reason why $H_{0.53}WO_3$/CdS possesses the perfect performance, while following Z-scheme photocatalytic mechanism may be the main factor to enhance photocatalytic performance.

3.3. Photocatalytic mechanism

Before proposing the mechanism for preparation of $H_{0.53}WO_3$/CdS,

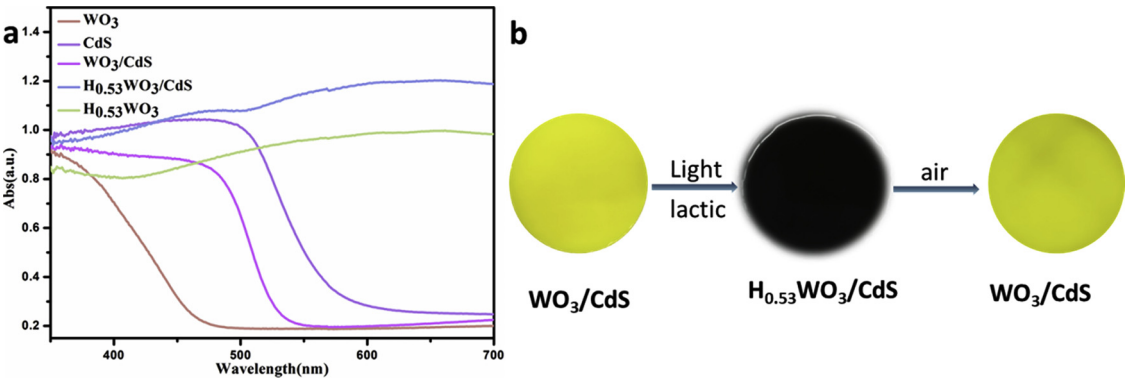

Fig. 6. (a) UV-vis diffuse reflectance spectrum of samples (b) Photograph of the WO_3/CdS suspensions before and after illumination.

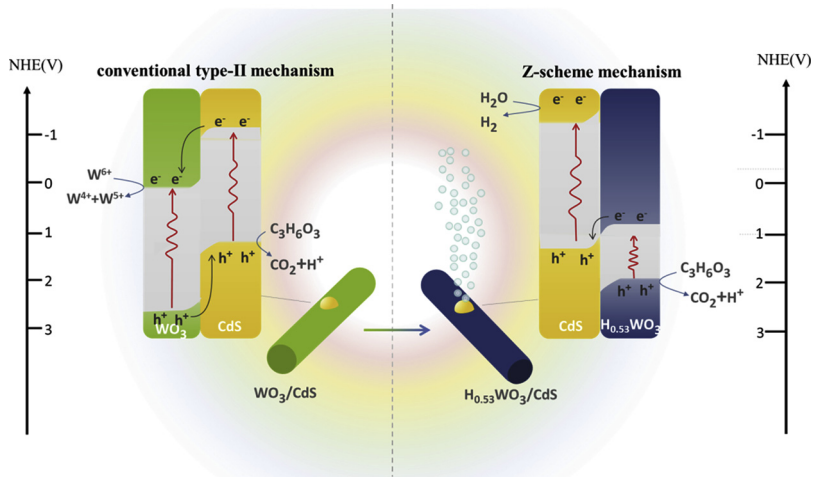

Fig. 8. Schematic illustration of the proposed mechanism for switching charge transfer from type-II to direct Z-scheme.

the energy level structure of $H_{0.53}WO_3$, WO_3 and CdS should be ascertained. According to the estimated value from data in inset of Fig. S4, the E_g of WO_3 and $H_{0.53}WO_3$ are 2.54 and 1.19 eV [42,43], respectively, while that of CdS is about 2.40 eV. As Fig. S5 shown, the VB of WO_3, CdS and $H_{0.53}WO_3$, obtained by XPS method, are 2.66, 1.27 and1.89 V, respectively. According to $E_{CB} = E_{VB}$-E_g, the CB of WO_3, CdS and $H_{0.53}WO_3$ are 0.12, -1.13 and 0.7 V, respectively.

On the basis of the above results, the proposed charge transfer mechanism of WO_3/CdS and $H_{0.53}WO_3$/CdS are proposed. As illustrated on the left of Fig.8, firstly, WO_3/CdS is illuminated under visible-light, both WO_3 and CdS can be excited and produce photogenerated electron–hole pairs at the same time. Since the potential difference of CB between of CdS and WO_3 is greater than that between CB of CdS and hydrogen production potential, it is quite possible for the carriers transfer in WO_3/CdS to follow the traditional type-II photocatalytic mechanism: the photoinduced electrons on the CB of CdS transfer to the CB of WO_3, while the photogenerated holes on the VB of WO_3 transfer to the VB of CdS. In this case, there are higher reducibility electrons on the CB of WO_3, and the followed processes can be happened.

$$W^{6+} + e^- \rightarrow W^{5+} \quad (1)$$

$$W^{5+} + e^- \rightarrow W^{4+} \quad (2)$$

$$WO_3 + xH^+ + xe^- \rightarrow H_xWO_3, \quad (3)$$

Then WO_3 is translated to $H_{0.53}WO_3$, while lactic acid as a sacrificial agent is oxidized by holes in CdS. The aforementioned process can be evidenced XRD analysis. As shown in Fig. S6a and S6b, it can be clear seen that the XRD patterns of individual CdS and WO_3 keep consistent before and after irradiation. According to this data, it is proved that pure WO_3 does not become colored tungsten bronze $H_{0.53}WO_3$ under visible light irradiation, while Fig.1 reveals that WO_3/CdS composite can successfully translate to $H_{0.53}WO_3$/CdS after photochromism. These data show that the sample WO_3 translates to $H_{0.53}WO_3$ only when CdS composited with WO_3, which indicates that the main reason why pure WO_3 can't be transformed is that the reducibility of electrons from the CB of WO_3 are not enough. Therefore, the above characterizations confirm the photocatalytic mechanism of WO_3/CdS is type-II.

While the mechanism for the photocatalytic H_2 production by $H_{0.53}WO_3$/CdS is proposed as the right of Fig.8. Both $H_{0.53}WO_3$ and CdS can be excited by illumination and produce photogenerated electron–hole pairs at the same time[3,43]. The photo-induced electrons on the CB of $H_{0.53}WO_3$ can recombine with holes located at the VB of CdS. In this case, the electrons with higher reducibility at CB of CdS can participate in photocatalytic process, leading to high performance of H_2 production, which follows Z-scheme mechanism. The illuminated open circuit potential (OCP) technique [44], which used to measure the Fermi level difference of samples, is applied to prove above mechanism and synthesis mechanism. As shown in Fig. S7, the measured ΔE_F difference ($\Delta E_F = E_F(WO_3)$-E_F(CdS)) is -0.13 eV in 0.5 M Na_2SO_4 solution, which means the Fermi level of WO_3 is much higher than that of CdS. Accordingly, in the WO_3/CdS system, the energy bands of WO_3 and CdS should bend upward and downward at the interface, respectively, which coincides with the proposed preparation mechanism (Fig.8). Surprisingly, the measured ΔE_F ($\Delta E_F = E_F(H_{0.53}WO_3)$-$E_F$(CdS)) is changed to + 0.59 eV, indicating the Fermi level of CdS is significantly higher than that of $H_{0.53}WO_3$, which may reverse the interfacial band bending, which means the interface charge transfer mode follows Z-scheme mechanism [18].

4. Conclusions

In summary, the charge transfer mode of WO_3/CdS can be switched from conventional type-II to Z-scheme by incorporating of hydrogen ions into WO_3/CdS. This work indicates that transformation in-situ of $H_{0.53}WO_3$/CdS composite is attributed to the type-II charge transfer of WO_3/CdS. Subsequently, Z-scheme photocatalytic mechanism plays its prominent roles in improving photocatalytic H_2 evolution performance gradually. $H_{0.53}WO_3$/CdS shows high photocatalytic performance for hydrogen production, which is more than 9 times greater than that of WO_3/CdS.

Acknowledgements

This work is supported by the National Natural Science Foundation of China (21473031, 21673041).

Appendix A. Supplementary data

Supplementary material related to this article can be found, in the online version, at doi:https://doi.org/10.1016/j.apcatb.2018.11.055.

References

[1] J. Wang, C.-j. Liu, ChemBioEng Reviews 2 (2015) 335–350.
[2] Q. Mi, Y. Ping, Y. Li, B. Cao, B.S. Brunschwig, P.G. Khalifah, G.A. Galli, H.B. Gray, N.S. Lewis, Journal of the American Chemical Society 134 (2012) 18318–18324.
[3] L. Zhang, W. Wang, S. Sun, D. Jiang, Applied Catalysis B: Environmental 168-169 (2015) 9–13.
[4] Y. Li, Z. Tang, J. Zhang, Z. Zhang, Applied Catalysis A: General 522 (2016) 90–100.
[5] L.J. Zhang, S. Li, B.K. Liu, D.J. Wang, T.F. Xie, ACS Catalysis 4 (2014) 3724–3729.
[6] X. Liu, Y. Yan, Z. Da, W. Shi, C. Ma, P. Lv, Y. Tang, G. Yao, Y. Wu, P. Huo, Y. Yan, Chemical Engineering Journal 241 (2014) 243–250.
[7] J. Jin, J. Yu, D. Guo, C. Cui, W. Ho, Small 11 (2015) 5262–5271.

[8] I. Aslam, C. Cao, M. Tanveer, M.H. Farooq, W.S. Khan, M. Tahir, F. Idrees, S. Khalid, RSC Adv. 5 (2015) 6019–6026.
[9] K. Villa, X. Domènech, U.M. García-Pérez, J. Peral, Catalysis Letters 146 (2015) 100–108.
[10] H. Kim, Y. Tak, K. Senthil, J. Joo, S. Jeon, K. Yong, Journal of Vacuum Science & Technology B: Microelectronics and Nanometer Structures 27 (2009) 2182.
[11] H. Li, Y. Zhou, L. Chen, W. Luo, Q. Xu, X. Wang, M. Xiao, Z. Zou, Nanoscale 5 (2013) 11933–11939.
[12] S. Kim, Y. Park, W. Kim, H. Park, Photochemical & photobiological sciences : Official journal of the European Photochemistry Association and the European, Society for Photobiology 15 (2016) 1006–1011.
[13] H. Li, W. Tu, Y. Zhou, Z. Zou, Advanced science 3 (2016) 1500389.
[14] A. Iwase, Y.H. Ng, Y. Ishiguro, A. Kudo, R. Amal, Journal of the American Chemical Society 133 (2011) 11054–11057.
[15] Y. Wang, H. Suzuki, J. Xie, O. Tomita, D.J. Martin, M. Higashi, D. Kong, R. Abe, J. Tang, Chemical reviews (2018).
[16] H. Li, Y. Gao, Y. Zhou, F. Fan, Q. Han, Q. Xu, X. Wang, M. Xiao, C. Li, Z. Zou, Nano letters 16 (2016) 5547–5552.
[17] K. Maeda, ACS Catalysis 3 (2013) 1486–1503.
[18] Z.-F. Huang, J. Song, X. Wang, L. Pan, K. Li, X. Zhang, L. Wang, J.-J. Zou, Nano Energy 40 (2017) 308–316.
[19] L. Shi, Z. Li, K. Marcus, G. Wang, K. Liang, W. Niu, Y. Yang, Chemical communications (2018).
[20] Z. Fang, S. Weng, X. Ye, W. Feng, Z. Zheng, M. Lu, S. Lin, X. Fu, P. Liu, ACS applied materials & interfaces 7 (2015) 13915–13924.
[21] M. Qiu, Y. Tian, Z. Chen, Z. Yang, W. Li, K. Wang, L. Wang, K. Wang, W. Zhang, RSC Advances 6 (2016) 74376–74383.
[22] S.G. Ullattil, P. Periyat, Journal of Materials Chemistry A 4 (2016) 5854–5858.
[23] B. Ma, M. Yue, P. Zhang, S. Li, R. Cong, W. Gao, T. Yang, Catalysis Communications 88 (2017) 18–21.
[24] X. Zhang, H. Tian, X. Wang, G. Xue, Z. Tian, J. Zhang, S. Yuan, T. Yu, Z. Zou, Materials Letters 100 (2013) 51–53.
[25] H. Zheng, J.Z. Ou, M.S. Strano, R.B. Kaner, A. Mitchell, K. Kalantar-zadeh, Advanced Functional Materials 21 (2011) 2175–2196.
[26] C. Guo, S. Yin, L. Huang, T. Sato, ACS applied materials & interfaces 3 (2011) 2794–2799.
[27] S. Kuba, P. Concepción Heydorn, R.K. Grasselli, B.C. Gates, M. Che, H. Knözinger, Physical Chemistry Chemical Physics 3 (2001) 146–154.
[28] B. Liu, D. Cai, Y. Liu, D. Wang, L. Wang, Y. Wang, H. Li, Q. Li, T. Wang, Sensors and Actuators B: Chemical 193 (2014) 28–34.
[29] T.F.J. S. H. Baeck, C. Bra¨ndli, and E. W. McFarland, 4 (2002).
[30] Y. Ikeuchi, H. Takatsu, C. Tassel, Y. Goto, T. Murakami, H. Kageyama, Angewandte Chemie 56 (2017) 5770–5773.
[31] C. Bechinger, E. Wirth, P. Leiderer, Applied Physics Letters 68 (1996) 2834–2836.
[32] R. Huang, Y. Shen, L. Zhao, M. Yan, Advanced Powder Technology 23 (2012) 211–214.
[33] Y. Liu, S. Shrestha, W.E. Mustain, ACS Catalysis 2 (2012) 456–463.
[34] T. He, J. Yao, Journal of Materials Chemistry 17 (2007) 4547.
[35] X. Jia, M. Tahir, L. Pan, Z.-F. Huang, X. Zhang, L. Wang, J.-J. Zou, Applied Catalysis B: Environmental 198 (2016) 154–161.
[36] X. Huang, K. Wang, Y. Wang, B. Wang, L. Zhang, F. Gao, Y. Zhao, W. Feng, S. Zhang, P. Liu, Applied Catalysis B: Environmental 227 (2018) 322–329.
[37] P. Chatchai, Y. Murakami, S.-y. Kishioka, A.Y. Nosaka, Y. Nosaka, Electrochimica Acta 54 (2009) 1147–1152.
[38] M. Remškar, J. Kovac, M. Viršek, M. Mrak, A. Jesih, A. Seabaugh, Advanced Functional Materials 17 (2007) 1974–1978.
[39] S.L. Wang, Y.L. Mak, S. Wang, J. Chai, F. Pan, M.L. Foo, W. Chen, K. Wu, G.Q. Xu, Langmuir : the ACS journal of surfaces and colloids 32 (2016) 13046–13053.
[40] M. Sun, N. Xu, Y.W. Cao, J.N. Yao, E.G. Wang, Journal of Materials Research 15 (2011) 927–933.
[41] H. Martinez, A. Benayad, D. Gonbeau, P. Vinatier, B. Pecquenard, A. Levasseur, Applied Surface Science 236 (2004) 377–386.
[42] F. Wang, C. Di Valentin, G. Pacchioni, The Journal of Physical Chemistry C 115 (2011) 8345–8353.
[43] Y. Xi, Q. Zhang, H. Cheng, The Journal of Physical Chemistry C 118 (2014) 494–501.
[44] T. Hisatomi, J. Kubota, K. Domen, Chemical Society reviews 43 (2014) 7520–7535.